Frozen Section Microautoradiography in the Study of Radionuclide Targeting: Application to Indium-111-Oxine-Labeled Leukocytes

Matthew R.B. Puncher and Philip J. Blower

Biological Laboratory, University of Canterbury and Nuclear Medicine Department, Kent and Canterbury Hospital, Canterbury, United Kingdom

The microscopic biodistribution of radioactivity in tissues is important in determining microdosimetry. This study addresses the use of frozen section microautoradiography in studying the sub-cellular distribution of ^{111}In in leukocytes labeled with ^{111}In-oxine. **Methods:** In conjunction with frozen section microautoradiography, computer image analysis methods were applied to the analysis and quantification of leukocyte sections and superimposed autoradiographs. Rapid cell fractionation was used to confirm the results. **Results:** The emulsion (Ilford K2) response was linear over the concentration range investigated (0–33 MBq ml^{-1}). Resolution of radionuclide distribution was better than 2 μm. The autoradiographs showed no dependence of radiolabel uptake on cell type. Classification of all cells into intervals according to grain density suggests an exponential rather than normal distribution, with approximately 50% of cells having little or no radiolabel. In any one sample, cells which were heavily labeled were approximately 10 times more likely to be found in aggregates (60% found in aggregates, mostly neutrophils) than cells which were not heavily labeled (6% found in aggregates); and the grain densities were at least twofold higher over nuclei than over cytoplasm. The last observation was confirmed by the rapid cell fractionation method which showed that approximately 57% of the total radioactivity was bound to nuclei. **Conclusion:** Frozen section microautoradiography is a practical and reliable approach to determining sub-cellular distribution of [111]In. The radiolabeling process causes aggregation of neutrophils. Uptake is not significantly dependent on cell type, but only a fraction of cells are appreciably labeled. The radioactive concentration in cell nuclei is at least two-fold higher than in cytoplasm. Microautoradiography can be used to provide distribution data as input into computer models for sub-cellular dosimetry.

Key Words: leukocytes; indium-111-oxine; microautoradiography

There is a growing interest in the biodistribution of radiopharmaceuticals at the cellular and sub-cellular level.

There are two reasons for this: (1) the need for knowledge of localization mechanisms; and (2) the need to consider microdosimetry for both diagnostic and therapeutic radionuclides. Several papers have shown that sub-cellular localization determines radiation doses to cell nuclei, and described mathematical and computer models of deposition of short-range particulate radiation at the microscopic level (1,2). These models will have only theoretical value, however, unless reliable information becomes available about the real microscopic distribution of radionuclide deposition in tissues and cells. This information is rarely available, even for radiopharmaceuticals in routine use.

Several methods have been advanced for the study of microscopic distribution of radiopharmaceuticals. Cellular fractionation by centrifugation of tissue homogenates suffers from the disadvantage that redistribution of radionuclide can occur during fractionation (3), and that it is unable to distinguish cytoplasmic from noncellular accumulation. Nonradionuclide methods, including secondary ion mass spectroscopy (SIMS) microscopic imaging (4), electron probe microanalysis and electron energy loss spectroscopy in the scanning electron microscope (5), are not sufficiently sensitive to detect elements at the carrier-free level. Microautoradiography, in which beta particles and secondary emissions such as Auger electrons are detected and localized, is more commonly used (6), and recently its application (in conjunction with computer image analysis) to microdosimetry has been described (7). Microautoradiography has the advantage that simultaneous visualization of tissue and superimposed autoradiograph is possible. However, it is most often used with fixed embedded tissue, raising the possibility of redistribution during sample preparation, especially with small molecular radiopharmaceuticals that are not firmly bound to a target. The alternative method of frozen section microautoradiography obviates this problem but has been surprisingly infrequently used (8). It has the additional advantage of very rapid sample preparation, and so can be conveniently used with short half-life radionuclides.

We have taken the latter approach in the study of radionuclide distribution in radiolabeled leukocytes, and we report new information on the distribution of ^{111}In in leukocytes labeled with ^{111}In-oxine. The microdosimetry is of

interest because of the high LET properties of Auger electrons emitted by ^{111}In and the known radiosensitivity of lymphocytes (9–11). The few studies on the sub-cellular distribution of ^{111}In in leukocytes labeled with ^{111}In-oxine are conflicting. Cell fractionation studies in neutrophils (12) and platelets (13) suggest that the radionuclide resides largely in the cytoplasm, while an electron microscope autoradiographic study in alveolar macrophages (14) suggests selectivity for cell nuclei.

MATERIALS AND METHODS

Preparation of Emulsions

All procedures on emulsions prior to fixation and development were performed in a dark room under a Ilford F904 safe-light. Large chromic acid-washed coverslips, mounted temporarily on microslides for convenient handling, were subbed in 0.5% gelatin and dried in a laminar flow cabinet. The slides were then dipped in molten (43°C) Ilford K2 nuclear emulsion (diluted 3:5 with distilled water), chilled on a leveled aluminum plate cooled with ice, dried on a leveled tray and stored at 4°C over desiccant.

Emulsion Response and Resolution

Indium-111-chloride (Amersham International plc, UK, 34 MBq, 0.1 ml) was mixed with 1 ml homogenized fresh rat liver, and the homogenate was assayed for radioactivity and withdrawn into a 0.5 ml syringe from which the Luer tip had been removed. The syringe was capped and placed in boiling water for 2 min to form a gel, which was then cooled to 4°C, ejected from the open end of the syringe, and frozen in Arcton 12 cooled with liquid nitrogen. The block so obtained was sectioned (5 μm) at -10°C. The frozen sections were transferred to emulsion coated coverslips and kept in the dark for 24 hr at -20°C. Similar preparations were made without radioactivity to determine chemographic effects yet none were observed. The slides were developed in Kodak D19 for 5 min and fixed in 30% sodium thiosulfate. The preparations were then stained with 1% eosin-Y to visualise the section edge, dehydrated and cleared. Finally, the emulsion coated coverslip was detached from the slide, inverted, and remounted in Histomount on a fresh slide.

To determine the sensitivity and linearity of response, the radioactive concentration of ^{111}In in the liver homogenate sections was varied by cutting and mounting the sections at different times. Grain density was determined over large areas (total 60,000 μm^2) and large numbers of grains (total 30,000) by use of computer image analysis. A UVP video camera attached to the Zeiss Universal microscope was interfaced with a PC-compatible digital image analysis system comprising a Synapse frame store (Synoptics, UK) and PC-IMAGES software (Foster Findlay Associates Ltd, UK). Dark field images, in which silver grains appear as bright objects, were recorded at a magnification of 400 × and analysed using PC-IMAGES. Silver grains were counted automatically over several fields of view (FOV) as follows. Threshold levels were selected to exclude homogenized tissue and include silver grains, and either the total area of grains or number of grains were determined. Grain numbers provide a more reliable measure of radioactivity since apparent grain areas are highly dependent on illumination conditions. Clusters of grains were corrected for by automated measurement of the area of each grain; grains larger than the maximum single grain area were thus identified automatically, and the number of grains in the cluster was calculated by dividing the cluster area by the mean grain area. Background

correction was made by determining grain density in regions distant from the section. The radioactive concentration was determined for each block before sectioning using a Vinten dose calibrator.

Resolution was crudely determined by examination of the edge of the liver homogenate sections. The FOV at the section edge was divided into 4 μm strips parallel to the edge, and the grain density in each strip was determined. A half-distance at the 11.1 MBq ml^{-1} radioactive concentration level (exposure time 24 hr) was estimated by plotting grain density in these strips versus distance from the section edge. Similar methods were applied to ^{125}I for comparison.

Autoradiography of ^{111}In-Leukocytes

Indium-111-oxine-labeled leukocytes were prepared by a routine method used clinically in our department (15). Sixty milliliter blood samples from normal volunteers were collected in heparinised syringes and erythrocytes precipitated with methyl cellulose. The supernatant, containing leukocytes, platelets and residual erythrocytes, was centrifuged to obtain a platelet-depleted leukocyte pellet, which was resuspended in 10 ml saline. Indium-111-oxine (Mallinckrodt Diagnostica, 37 MBq, ca. 1.4 ml including TRIS buffer) was added dropwise to this suspension. After 10 min, the suspension was centrifuged and the pellet resuspended in platelet-depleted plasma (2 ml). This suspension was withdrawn into a 4-mm diameter thin-walled stainless steel tube using a rubber plunger, and immersed in coolant as described for the liver paste standards. The frozen cell suspension was ejected and freeze-mounted with OCT to the cryotome chuck. Sections were cut (6 μm) and autoradiographed (24 hr exposure) as described for the liver paste standards. Immediately after exposure and before development, the cells were fixed with 4% formaldehyde in phosphate buffer, pH 7.4. The emulsions were then developed and fixed, and the sections were stained with Caruzzi's haematoxylin and 0.05% eosin. The same procedure was applied to a control sample, in which the ^{111}In-oxine had been allowed to decay for several months. In a second control, the same procedure was again followed but omitting the addition of ^{111}In-oxine solution altogether.

Image Analysis. The sections were viewed with a 40× objective. Silver grain images were stored digitally using dark field illumination, and the same area was imaged with bright field to record digitally the section itself. Several FOV were digitised in this way for later analysis. Regions of interest (ROI) were drawn around all cells in the digital images, and around nucleus fragments, close to the focal plane of the silver grains. Areas of these ROI were calculated using a pixel size factor obtained by calibration with a stage graticule. Background ROI were also sampled in each FOV. Estimates of fractional cell volumes occupied by nuclei were obtained from the following relation: fractional nuclear volume (%) = [(nuclear area)$^{3/2}$/(cell area)$^{3/2}$] × 100%. The ROI were used as a template, superimposed on the dark field images, for determining grain numbers and densities (grains/100 μm^2) in each ROI.

Cell Fractionation. The rapid method described by Hymer and Kuff (16) was used to separate nuclei from cytoplasm in labeled cell suspensions. Labeled leukocyte pellets (prepared as described above) were freed of erythrocyte contamination by resuspension in lysis buffer (2 ml of 155 mM NH$_4$Cl, 10 mM KHCO$_3$, 0.1 mM ethylenediaminetetraacetic acid) for 7–8 min at 0–4°C. The leukocytes were then pelleted at 150 g for 7 min, resuspended in 2 ml 0.25 M sucrose/3 mM MgCl$_2$, and broken with 10 strokes

of a Dounce homogeniser. The suspension was then centrifuged (800 g, 10 min) and the pellet resuspended in 0.25 M sucrose/3 mM MgCl$_2$/0.1% Triton X-100 detergent. The suspension was centrifuged (400 g, 10 min) to obtain a nuclear pellet. The pellet and supernatant were assayed in a Vinten ionisation chamber. The Triton X-100 step was repeated and the pellet and supernatant counted again. Microscopic examination (40 × phase contrast) was used to verify the composition of each fraction, since there was insufficient material to carry out enzyme assays.

Statistical Analysis

Throughout the text, uncertainties are given as ± estimated s.d. Various statistical tests were applied according to the circumstances. Correlation of cell type with grain density was tested using a Kolmogorov-Smirnov test since the grain density distribution among all types of cells was non-normal. Correlation between the two numerical variables of grain density and probability of aggregation was tested by calculating a Kendall rank-correlation coefficient. For comparison of aggregation in labeled and unlabeled cell samples, the variation in degree of aggregation between similarly prepared samples, whether labeled or unlabeled, was assumed to be normal. The grain density difference between nuclei and cytoplasm was tested as follows: the expected number of grains over the nucleus (assuming uniform distribution of intracellular grains) was calculated as the number of grains over the cell multiplied by the fractional cell area occupied by the nucleus, and was compared with the observed number with a chi square test.

RESULTS

Autoradiography Standards

Estimates of sensitivity and resolution of the emulsion were made using frozen sections of rat liver homogenate. This medium was compared with other materials such as OCT (8) (a polyethylene glycol based embedding medium) and coagulated egg albumin. The medium sectioned and adhered well to the emulsion while frozen; aqueous solutions of radionuclides were readily and evenly dispersed in it; and the section edge could be readily visualized by staining.

In the range of radioactive concentrations and exposure times examined (up to 33 MBq ml^{-1} for up to 24 hr), the emulsion response was linear (r = 0.998, Fig. 1). The sensitivity (number of silver grains formed per disintegration occurring in the same area during the exposure time, expressed as a percentage, for the stated section thickness) of 4.1% compares well with that for ^{125}I (6.5%), which was determined for comparison since it has been more widely used in microautoradiography. Because of the short range of the Auger electrons emitted (17), the apparent sensitivity will increase as section thickness diminishes from 5 μm.

The energy of the emitted electrons also affects the resolution (defined as the distance from the source edge at which the grain density falls to half its average value above the source). The standards demonstrate that the location of radioactivity in these frozen sections can be determined to within 2 μm (Fig. 2). Because of the unevenness in the edge over which the response was determined, no attempt was made to define resolution below 2 μm. Thus, 2 μm repre-
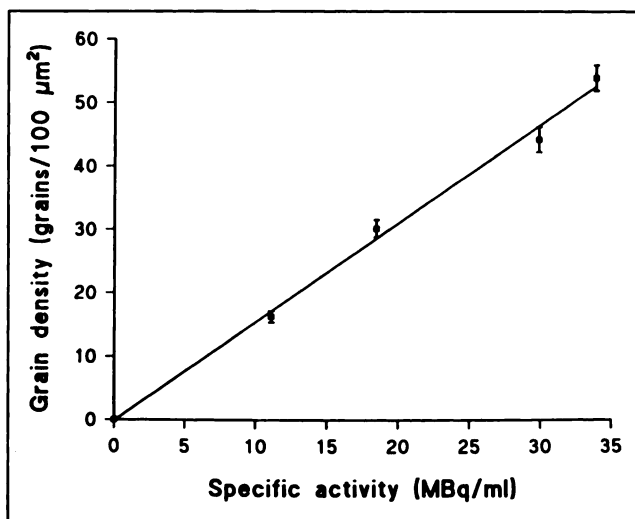

FIGURE 1. Response of Ilford K2 emulsion to ^{111}In. Grains per unit area (corrected for background) shown as a function of radioactive concentration in tissue paste section. Emulsion thickness 1 μm, section thickness 5 μm and exposure time 24 hr.

sents a worst estimate, and compares well with that obtainable with ^{125}I, which was also found to be better than 2 μm by this method.

Labeled Leukocyte Autoradiography

Visual inspection of the leukocyte autoradiographs (an example is shown in Fig. 3) creates the impression that cells fall into two categories: labeled and unlabeled. Quantitative analysis of grain density over randomly selected cells shows that this is an oversimplified impression. The distribution of grain density values for randomly selected cells, shown in Fig. 4, appears exponential rather than normal as might have been intuitively expected, and confirms that there is a high proportion of cells with little or no label. Cells with grain densities below 10–15 per μm^2 (46% ± 6% of 2064 leukocytes counted) gave no visual
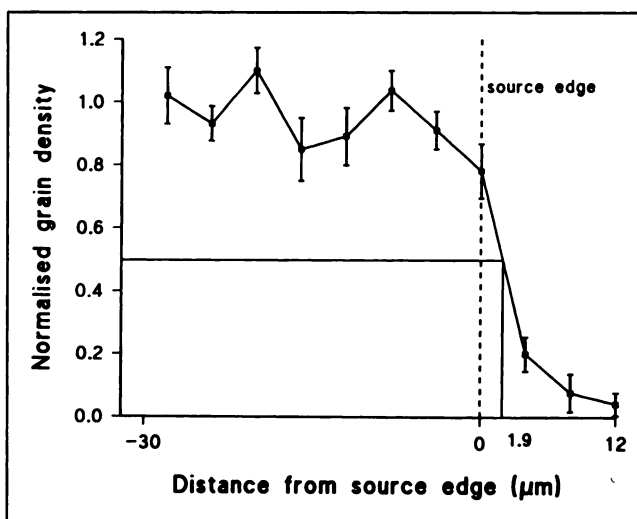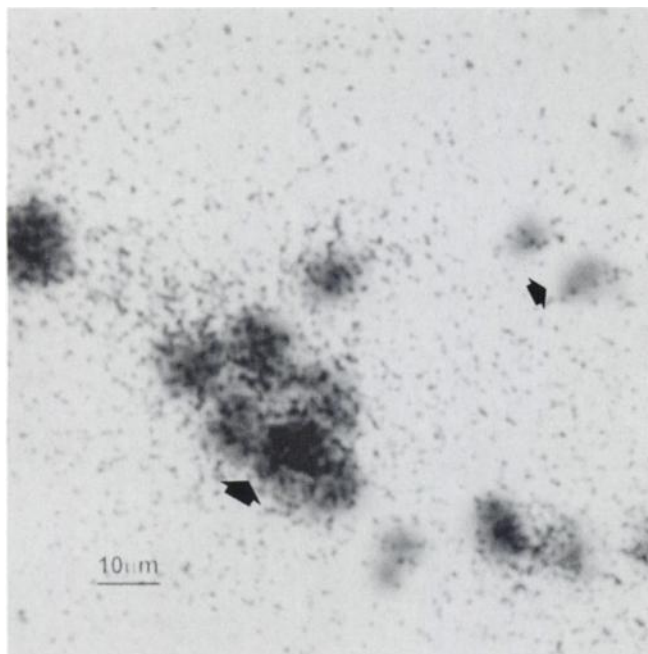

FIGURE 2. Plot of grain density as a function of distance from the edge of a uniformly labeled section of liver paste.

FIGURE 3. Autoradiographs of ^{111}In-oxine labeled leukocytes. Some cells are heavily labeled (large arrow) while others (small arrow) apparently unlabeled. Heavily labeled cells are aggregated, while unlabeled cells are not.

impression of being labeled, and by inspection were assigned to the unlabeled category. It was possible to distinguish neutrophils, eosinophils, and mononuclear cells in the sections but not to identify sub-types of mononuclear cells. The mean grain density ($100~\mu m^{-2}$) over granulocytes was 44.1 ± 46.4 and over mononuclear cells was 33.4 ± 45.6. The difference is not significant according to a Kolmogorov-Smirnov test ($p < 0.3\%$).
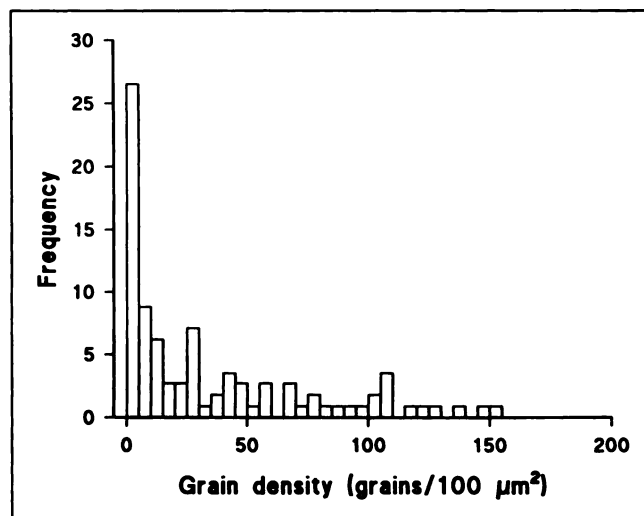
FIGURE 4. Histogram showing distribution of grain densities over cells labeled by the normal labeling procedure. An unexpectedly large proportion of cells show little or no labeling. The threshold at which cells can be visually identified as labeled is 10–15 grains/100 μm^2.

There was a strong tendency of labeled neutrophils (but not unlabeled neutrophils in the same slide) to form aggregates. In labeled samples, of the labeled cells 60% ± 14% (essentially, all the neutrophils) were in aggregates of two or more cells (up to 10, typically 4–5 in sections; this corresponds to a typical three-dimensional cluster size of about 10 cells), while of the unlabeled cells, only 6% ± 2% were in aggregates. There was a close correlation (Kendall coefficient 0.745; highly significant, $p < 1\%$) between grain density and the probability of aggregation. Almost all of the aggregated cells were neutrophils. Overall, 32% ± 4% of the total cell population in the labeled sample were aggregated, while in the samples in which addition of ^{111}In-oxine was omitted completely, only 6.7% appeared in aggregates (outside 95% confidence limit for the normal distribution in the labeled population), and in samples in which decayed ^{111}In-oxine was used, 26% (within 95% confidence limit) were aggregated.

Inspection of the autoradiographs of very heavily labeled cells suggests that the radionuclide is primarily deposited in cell nuclei of both granulocytes and mononuclear cells. Under these conditions, nuclei could not be clearly delineated since they were obscured by silver grains. By using image analysis to delineate nuclear and extranuclear ROI for less heavily labeled cells, the selectivity could be quantified. Results are summarized in Table 1. Grain densities were determined over nuclei and cytoplasm of 15 granulocytes and 11 mononuclear cells: 65% ± 8% of grains over mononuclear cells and 65% ± 9% over granulocytes were found over nuclei or nuclear fragments. By using image analysis to determine areas of ROI, these values were used to calculate individual nuclear-to-cytoplasmic grain density ratios. The mean ratio was 2.23 ± 1.07 for granulocytes and 2.24 ± 0.67 for mononuclear cells. Chi square analysis showed that the difference between the observed nuclear grain density and that expected on the basis of uniform distribution of intracellular activity was highly significant ($p < 0.1\%$).

Cell Fractionation

To validate the microautoradiographic observation of selectivity for nuclei, a rapid cell fractionation method was used (16). After homogenisation, cell-free nuclei were isolated by treatment of the homogenate with 0.1% Triton X-100. After the first treatment, the nuclear pellet contained 57% ± 4% of the radioactivity and 91% of the visible nuclei were cell/cytoplasm-free (by phase contrast microscopy). After the second treatment, the nuclear pellet contained 47% ± 9% of the radioactivity, while 96% of the visible nuclei were cell/cytoplasm-free. The first of these is the more reliable, since although the pellet is significantly contaminated with cytoplasmic debris, the second has lost more radioactivity than can be accounted for by the increase in purity, suggesting that the treatment causes significant lysis or loss of nuclei, or leakage of radioactivity from them. This suggests that there is significantly greater radioactive concentration inside nuclei than outside them,

502

Parameter	Neutrophils	Eosinophils	Mononuclear cells
Relative cell volume (from sectional areas)	1.0	1.16	0.58
Mean fractional nuclear volume (%)	39 (12)	21 (11)	44 (15)
Mean nuclear: cytoplasmic grain density ratio*			2.24 (0.67)
Typical composition of leukocytes (%)	60	5	35
Calculated bulk nuclear volume (%)	39	39	39
Calculated bulk nuclear activity (%)	59	59	59
Found bulk nuclear activity (%) by fractionation	57 (4)[†]	57 (4)[†]	57 (4)[†]
	47 (9)[‡]	47 (9)[‡]	47 (9)[‡]

*Nuclear-cytoplasmic grain density ratios were not determined separately for eosinophils and neutrophils.
[†]1st Triton wash.
[‡]2nd Triton wash.

since the nuclei occupy a much smaller mean fraction of the cell volumes than 57%. We estimate from image analysis that the mean fractional cell volume occupied by the nucleus is approximately 39% ± 12% for neutrophils, 21% ± 11% for eosinophils and 44% ± 15% for mononuclear cells.

DISCUSSION

Microautoradiography, though not frozen section microautoradiography, has been employed by others in studying the microscopic distribution of ^{111}In-labeled immunoglobulin in abscesses (18), various ^{111}In radiopharmaceuticals in normal animal tissues (19), and ^{111}In-oxine in alveolar macrophages (the latter by electron microscope autoradiography) (14). The linearity of the emulsion response to uniformly labeled tissue confirms that grain density in the autoradiograph provides a direct measure of the radioactivity in the uppermost layers of the section (in immediate contact with the emulsion). A concentration of 33 MBq/ml, the highest level examined in the standards in this study, does not cause saturation with an exposure time of 24 hr. A linear relationship was found also by Morrel et al. (18), using Kodak NTB-2 emulsion and 1 μm sections. The resolution is 2 μm or better. Morrel et al. showed that resolution of 0.6 μm (by the same definition) is possible for ^{111}In (18). This value was obtained by a similar method to ours, and suffers from similar uncertainties because the width (2.2 μm) of the strips in which grains were counted was large compared to the true resolution attainable. Both values show that the secondary electron emissions are suitable for microautoradiography, and our results confirm that the frozen section approach is able to immobilise radioactivity at the microscopic level during exposure. The resulting resolution is sufficient to distinguish radioactivity associated with nuclei, cytoplasm, and plasma membrane, as well as with different cells.

Previous attempts to determine the sub-cellular distribution of ^{111}In in ^{111}In-oxine labeled cells have been made using cell fragmentation and fractionation methods [applied to neutrophils (12) and platelets (13)] and electron microscope microautoradiography (of alveolar macrophages (14)). The cell fractionation approach led to the conclusion that 80% of the postnuclear supernatant (12) radioactivity in neutrophils was associated with macromolecules whose distribution on isopycnic centrifugation was similar to that of lactate dehydrogenase, indicative of cytoplasmic localisation. The percent recovery of radioactivity was 75%; we assume the remaining 25% was present in the nuclear pellet. As the authors pointed out (12), the interpretation of these results requires caution, it is impossible to show that the radionuclide does not become significantly redistributed during the fractionation experiment. The electron microscope autoradiography approach led to the conclusion that the radioactive concentration is approximately 4–5-fold higher in the nuclei of alveolar macrophages than in their cytoplasm. With the extensive preparation including fixing and embedding prior to sectioning, it is questionable whether the observed distribution is a true reflection of the distribution in freshly labeled cells. The frozen section approach taken in the present study, while undoubtedly having its own disadvantages (relatively poor resolution and histological quality), minimizes the possibility of redistribution. Our microautoradiographic results suggest a radioactive concentration ratio of 2.2:1 for nucleus: cytoplasm for all cell types. The observed grain densities suggest that at least 52% of the cellular radioactivity is intranuclear for neutrophils (assuming a mean fractional cell volume of 39% occupied by nuclei, a value estimated from our own sections), 64% for mononuclear cells (mean fractional nuclear volume 44%) and 37% for eosinophils (mean fractional nuclear volume 21%). Assuming the leukocyte population comprises approximately 60% neutrophils, 35% mononuclear cells and 5% eosinophils and the relative volumes of the cell types are 1.16:1.0:0.58 (eosinophils:neutrophils:mononuclear cells; determined from cross-sectional area measurements), then in the cell fractionation experiment we should expect to find 59% of the radioactivity in the nuclear pellet. This is in reasonable agreement with the observed result (57% after one treatment with Triton X-100). The cell frac-

tionation method used here was selected because it is simple and rapid, and the purpose was simply to distinguish nuclear from non-nuclear fractions without further fractionation.

The determination of quantitative subcellular radioactivity distribution, coupled with recent developments in mathematical modeling of sub-cellular dosimetry, provides the opportunity to calculate estimates of radiation doses to cell nuclei from high-LET electron emissions. Combination of our results with the lymphocyte dosimetry model of Faraggi et al. (2) suggests that the cell nuclei receive a dose rate that is roughly 2-fold higher than the cytoplasm. An absolute dose rate could be calculated from knowledge of the absolute cellular total radioactivity. The selective nuclear targeting may be correlated with severe chromosomal aberrations seen in lymphocytes labeled with ^{111}In-oxine at clinically used concentrations (but not seen when decayed ^{111}In-oxine was used) (11). Wagstaff (9) estimates the risk of malignancy resulting from these detrimental effects as minimal because of the relatively small number of reinjected labeled lymphocytes and their low probability of proliferation. The nuclear targeting is probably inconsequential for clinical use of ^{111}In-oxine-labeled leukocytes because of this low risk. In proliferative tissues, however, it is likely that nuclear targeting by radionuclides is an important risk factor for malignancy as a result of imaging procedures using Auger-emitting nuclides (e.g., ^{99m}Tc, ^{111}In). Frozen section microautoradiography provides a simple and reliable method of determining the extent of this nuclear targeting.

It was possible to obtain information not only on the subcellular distribution of radioactivity but also on the population distribution and its effects. There are two significant findings: a high proportion of unlabeled cells and a correlation of aggregation with grain density. The unexpected non-normal distribution of radiolabel among the leukocyte population (Fig. 4) was unrelated to cell type, suggesting a nonspecific mechanism. This contrasts with our related studies on leukocytes labeled with ^{99m}Tc-HMPAO, which show strong eosinophil selectivity. The most likely cause of the high proportion of unlabeled cells is that accumulation of radiolabel by cells is rapid, and dropwise addition of the radiolabel to the cell suspension results in rapid depletion of free ^{111}In-oxine by the first cells to come into contact with it, leaving remaining cells unlabeled.

The correlation between autoradiographic grain density and aggregation of the cells is evident from Figure 5. Essentially, within a given preparation, unlabeled neutrophils (those which have been treated with ^{111}In-oxine but which have accumulated little or no radioactivity) do not aggregate, while labeled neutrophils do. Mononuclear cells, even labeled ones, do not aggregate to a significant extent. Aggregation is one manifestation of activation of neutrophils (20–22). The commonly observed transient lung accumulation of ^{111}In-labeled granulocytes may at least in part be due to aggregation of neutrophils (23). The autora-
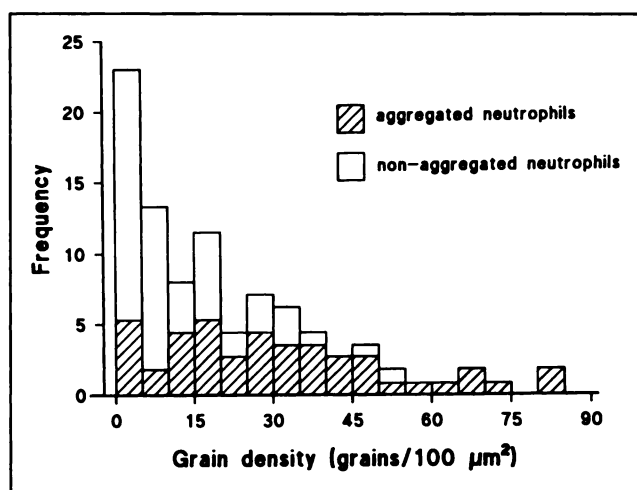

FIGURE 5. Relation between labeling and aggregation determined by autoradiography. The total of the shaded and unshaded areas represents all neutrophils. At grain densities above 50 grains/100 μm^2, essentially all neutrophils are aggregated.

diographs show that the majority of the radioactivity is associated with aggregates large enough to be trapped in the lung capillary bed. The control experiments, using untreated cells and cells treated with decayed ^{111}In-oxine, suggest that the aggregation is due neither to the absorbed radioactivity, nor to the adverse effects of the isolation and washing procedure, but to some chemical component of the ^{111}In-oxine solution, perhaps oxine or In-oxine. Further evidence for a specific chemical effect is found by comparison with analogous studies of leukocytes labeled with ^{99m}Tc-HMPAO, where no significant aggregation was observed. It is to be expected that cells which show the highest labeling will have the highest tendency to aggregate, despite lack of a direct radioactivity effect, since these cells will have been exposed to the highest levels of added chemicals before complete mixing has occurred.

CONCLUSION

Frozen section microautoradiography is an attractive method of studying the biodistribution of radiopharmaceuticals at the microscopic level. It offers unparalleled confidence that the radioactivity distribution in the object during exposure is not altered by chemical processing, at the expense of histological quality and resolution compared to embedded section. Despite this limitation, resolution of better than 2 μm is attainable. Computer image analysis is a useful, perhaps indispensable adjunct to this method, offering the ability to process large grain numbers and accurately determine grain densities. Application of the methods to ^{111}In-labeled leukocytes showed selectivity of radiolabel for cell nuclei, non-uniform and non-normal distribution of radiolabel among the population, lack of selectivity of radiolabel for different cell types, and aggregation of neutrophils caused by a chemical effect during the labeling process. Finally, and perhaps most significantly, wider application of the methods described with a wider variety

504

of radionuclides (24) above will permit estimation of real sub-cellular distribution of radiation dose from diagnostic and therapeutic radionuclides in a variety of clinical situations.

ACKNOWLEDGMENTS

REFERENCES

1. Siegel JA, Stabin MG. Absorbed fractions for electrons and beta particles in spheres of various sizes. *J Nucl Med* 1994;35:152–156.
2. Farraggi M, Gardin I, de Labriolle-Vaylet C, Moretti J-L, Bok BD. The influence of tracer localization on the electron dose rate delivered to the cell nucleus. *J Nucl Med* 1994;35:113–119.
3. Sheridan PJ, Buchanan JM, Anselmo VC, Martin PM. Equilibrium: the intracellular distribution of steroid receptors. *Nature* 1979;282:579–582.
4. Fourre C, Halpern S, Jeusset J, Clerc J, Fragu P. Significance of secondary ion mass spectroscopy microscopy for technetium-99m mapping in leukocytes. *J Nucl Med* 1992;33:2162–2166.
5. Trebbia P, Bonnet N. EELS elemental mapping with unconventional methods. I. Theoretical basis—image analysis with multivariate statistics and entropy concepts. *Ultramicroscopy* 1990;34:165–178.
6. Rogers AW. *Techniques of microautoradiography*, 3rd ed. New York: Elsevier North Holland Biomedical Press; 1979.
7. Humm JL, Machlis RM, Bump K, Cobb LM, Chin LM. Internal dosimetry using data derived from autoradiographs. *J Nucl Med* 1993;34:1811–1817.
8. Willis KW, Martinez DA, Hedley White ET, et al. Renal localisation of 99mTc stannous glucoheptonate and 99mTc-stannous dimercaptosuccinate in the rat by frozen section autoradiography. *Radiat Res* 1977;69:475–488.
9. Wagstaff J. Lymphocyte migration studies in man. In: Thakur M, ed. *Radiolabeled cellular blood elements* (NATO ASI series). New York: Plenum Press; 1985:319–342.
10. Sprent J. Migratory properties and radiosensitivity of lymphocytes. In: Thakur M, ed. *Radiolabeled cellular blood elements* (NATO ASI series). New York: Plenum Press; 1985:31–50.
11. ten Berg RJ, Natarajan AT, Hardeman MR, van Royen EA, Schellekens PThA. Labeling with indium-111 has detrimental effects on human lymphocytes: concise communication. *J Nucl Med* 1983;24:615–620.
12. Thakur ML, Segal AW, Louis L, Welch MJ, Hopkins J, Peters TJ. Indium-111-labeled cellular blood components: mechanism of labeling and intracellular location in human neutrophils. *J Nucl Med* 1977;18:1020–1024.
13. Hudson EM, Ramsey RB, Evatt BL. Subcellular localization of indium-111 in indium-111-labeled platelets. *J Lab Clin Med* 1981;97:577–582.
14. Davis HH, Senior RM, Griffin GL, Kuhn C. Indium-111-labeled human alveolar macrophages and monocytes: function and ultrastructure. *J Immunol Methods* 1980;36:99–107.
15. Mountford PJ, Kettle AG, O'Doherty MJ, Coakley AJ. Comparison of technetium-99m-HM-PAO leukocytes with indium-111-oxine leukocytes for localizing intraabdominal sepsis. *J Nucl Med* 1990;31:311–315.
16. Hymer WC, Kuff EL. Isolation of nuclei from mammalian tissues through the use of Triton X-100. *J Histochem Cytochem* 1964;12:359–363.
17. Weber DA, Eckerman KF, Dillman LT, Ryman JC. *MIRD: radionuclide data and decay schemes*. New York: Society of Nuclear Medicine; 1989.
18. Morrel EM, Tompkins RG, Fischman AJ, et al. Autoradiographic method of quantitation of radiolabeled proteins in tissues using indium-111. *J Nucl Med* 1989;30:1538–1545.
19. Jönsson B-A, Strand S-E, Bengt SL. A quantitative autoradiographic study of the heterogeneous activity distribution of different indium-111-labeled radiopharmaceuticals in rat tissues. *J Nucl Med* 1992;33:1825–1833.
20. Hammerschmidt DE, Harris PD, Wayland JH, Craddock PR, Jacob HS. Complement-induced granulocyte aggregation in vivo. *Am J Pathol* 1981; 102:146–150.
21. Rochon YP, Frojmovic MM. A model for the recruitment of neutrophils at sites of inflammation. Physiological relevance of in vivo neutrophil aggregation. *Med Hypoth* 1992;38:132–138.
22. Berliner S, Aronson M. The phenomenon of leukergy (leukocyte adhesiveness/aggregation): a powerful investigative tool and a sensitive indicator of inflammation, trauma and stress. *Israel J Med Sci* 1991;27:164–172.
23. Peters AM, Saverymuttu SH, Lavender JP. Granulocyte kinetics. In: Thakur M, ed. *Radiolabeled cellular blood elements* (NATO ASI series). New York: Plenum Press; 1985:285–303.
24. Puncher MRB, Blower PJ. Radionuclide targeting and dosimetry at the microscopic level: the role of microautoradiography. *Eur J Nucl Med* 1994; 21:1347–1365.